Supplementary Information

Inertial focusing and zeta potential measurements of single-nanoparticles using octet-nanochannels

Shohei Kishimoto[1,*], Makusu Tsutsui[1,*], Kazumichi Yokota[2], and Masateru Taniguchi[1]

[1] *The Institute of Scientific and Industrial Research, Osaka University, 8-1 Mihogaoka, Ibaraki, Osaka 567-0047, Japan.*

[2] *National Institute of Advanced Industrial Science and Technology, Takamatsu, Kagawa 761-0395, Japan*

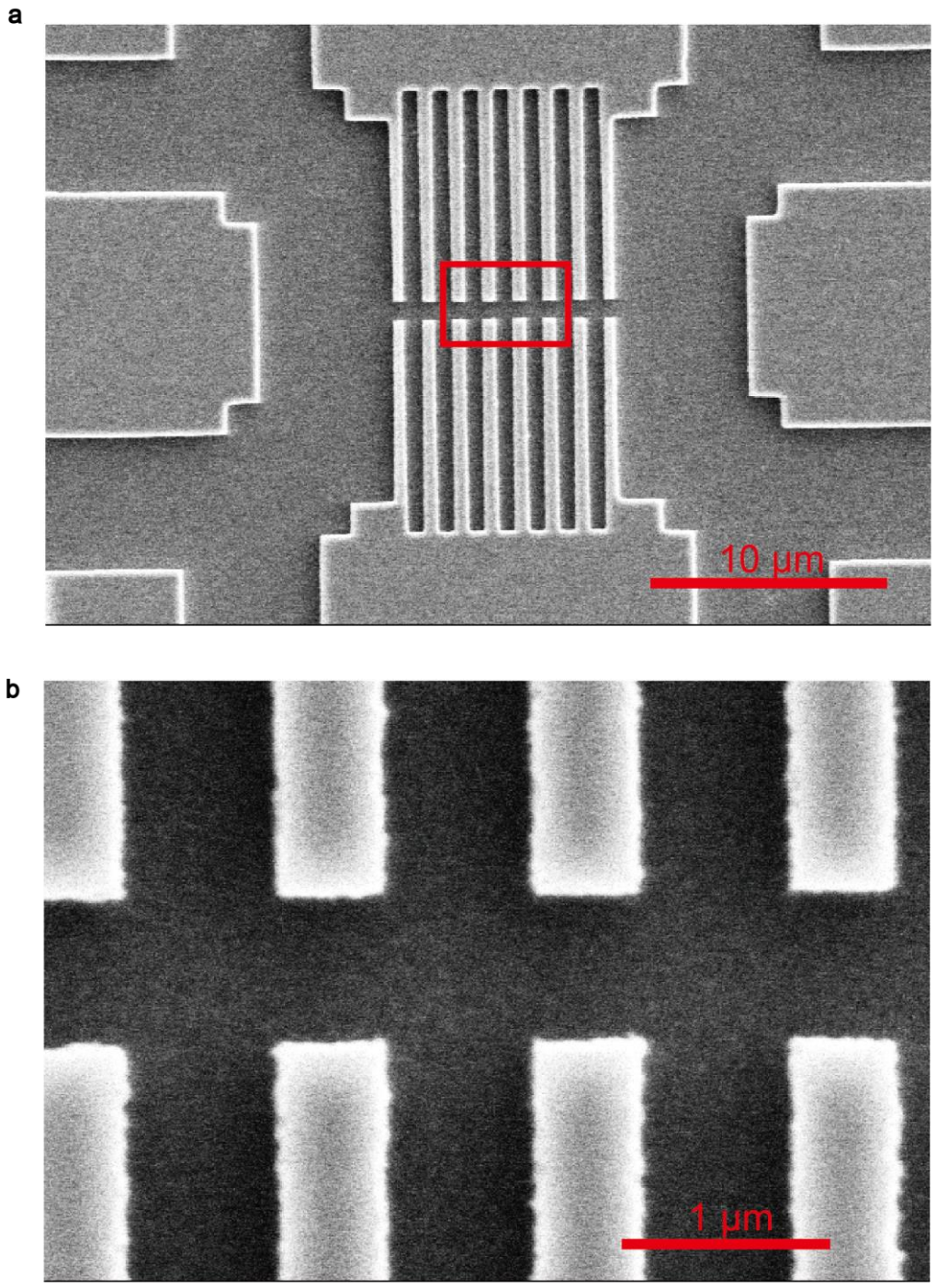

Figure S1. SEM image of an octet nanochannel. a, Scanning electron micrograph taken from the top. **b,** A magnified view of the red rectangle region in (a).

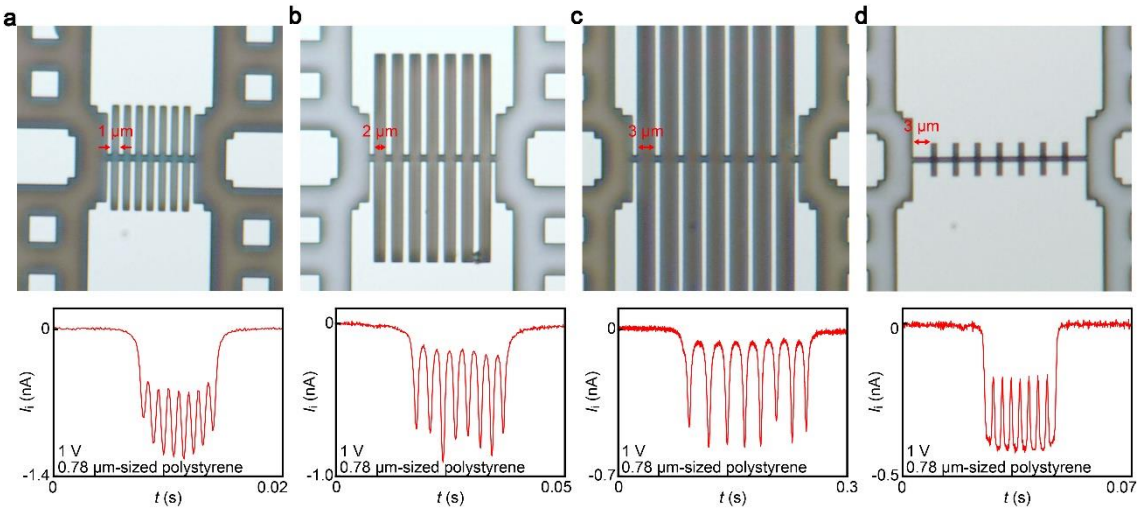

Figure S2. a-c, Octet nanochannels of length 1 μm with inter-channel gaps of 1 μm (a), 2 μm (b), and 3 μm (c). Typical resistive pulse signals were shown below each image. The signals demonstrate larger current up/downs upon particle translocation in the octet channels with wider inter-channel gap space. This can be explained by the decrease in the resistance at the gaps between the channels that indicates weaker electric field there. Meanwhile, the heights of sub-pulses were observed to scatter more with increasing the channel distance, which is presumably due to the more random incident angles of the particles at the capture stages that led to varying off-axis effects on the resistive pulse heights.[S1] Since we wanted to have negligible influence of Brownian motions at the gap space for the sake of more regular translocation dynamics to accurately estimate the particle zeta potential, we chose the inter-channel distance to be as short as the length of each channel. **d,** Meanwhile, since the longer channels led to lower signal-to-noise ratio (channel length is 3 μm in this case that led to the weaker resistive pulse signals), we selected the relatively short channel structures.

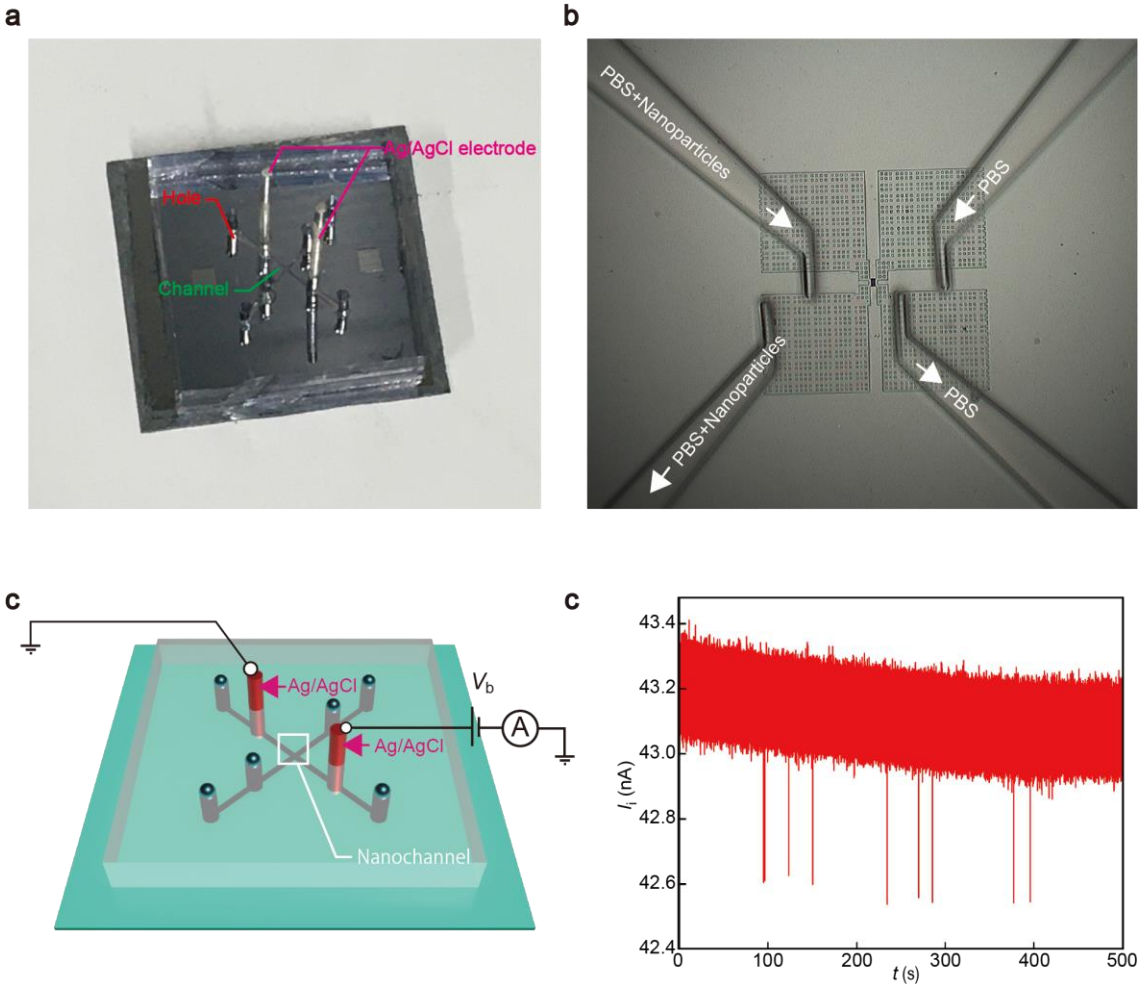

Figure S3. Measurement set up for resistive pulse detections of single nanoparticles. **a,** Photograph displaying the octet nanochannel chip sealed by a PDMS block from the top. The six holes punched in the PDMS were used as inlets and outlets to flow nanoparticle dispersion solution into the nanochannel. The other two holes were utilized for placing Ag/AgCl rods for the cross-channel ionic current measurements. **b,** A close view showing the microchannels in the PDMS and the SiO_2/Si chip. Through the holes in the PDMS, PBS containing polystyrene nanoparticles was flown at one side of the nanochannel, while only PBS was injected at the other side. **c,** Schematic model of the device set up. **d,** A partial ionic current (I_i) versus time (t) curve obtained for the 460 nm-sized amino-modified polystyrenes.

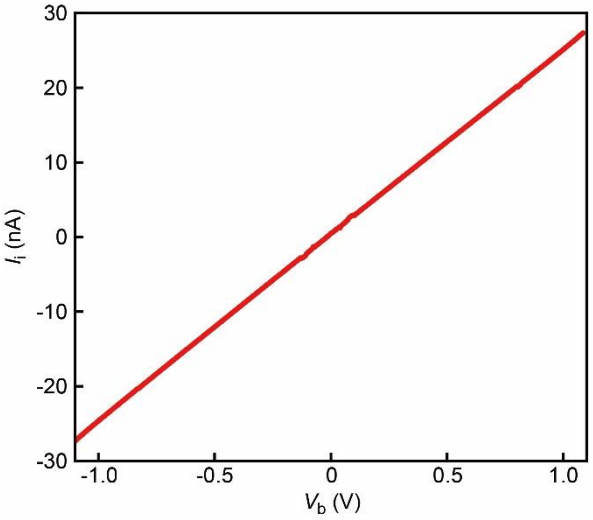

Figure S4. The ionic current I_i through the octet nanochannel in 1 x PBS plotted as a function of the applied voltage V_b.

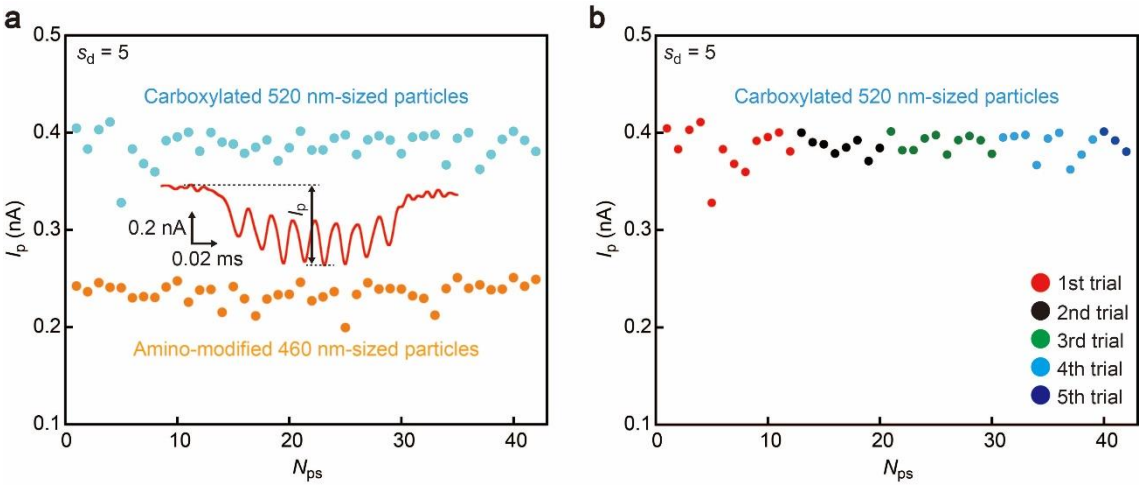

Figure S5. a, Resistive pulse heights I_p of 460 nm-sized amino-modified (orange) and 520 nm-sized carboxylated polystyrene beads (skyblue) plotted as a function of the number of pulses N_{sp}. I_p is defined as the height of the fifth sub-pulse as shown in the inset. **b,** Variations in I_p of the carboxylated particles among the five trials of measurements.

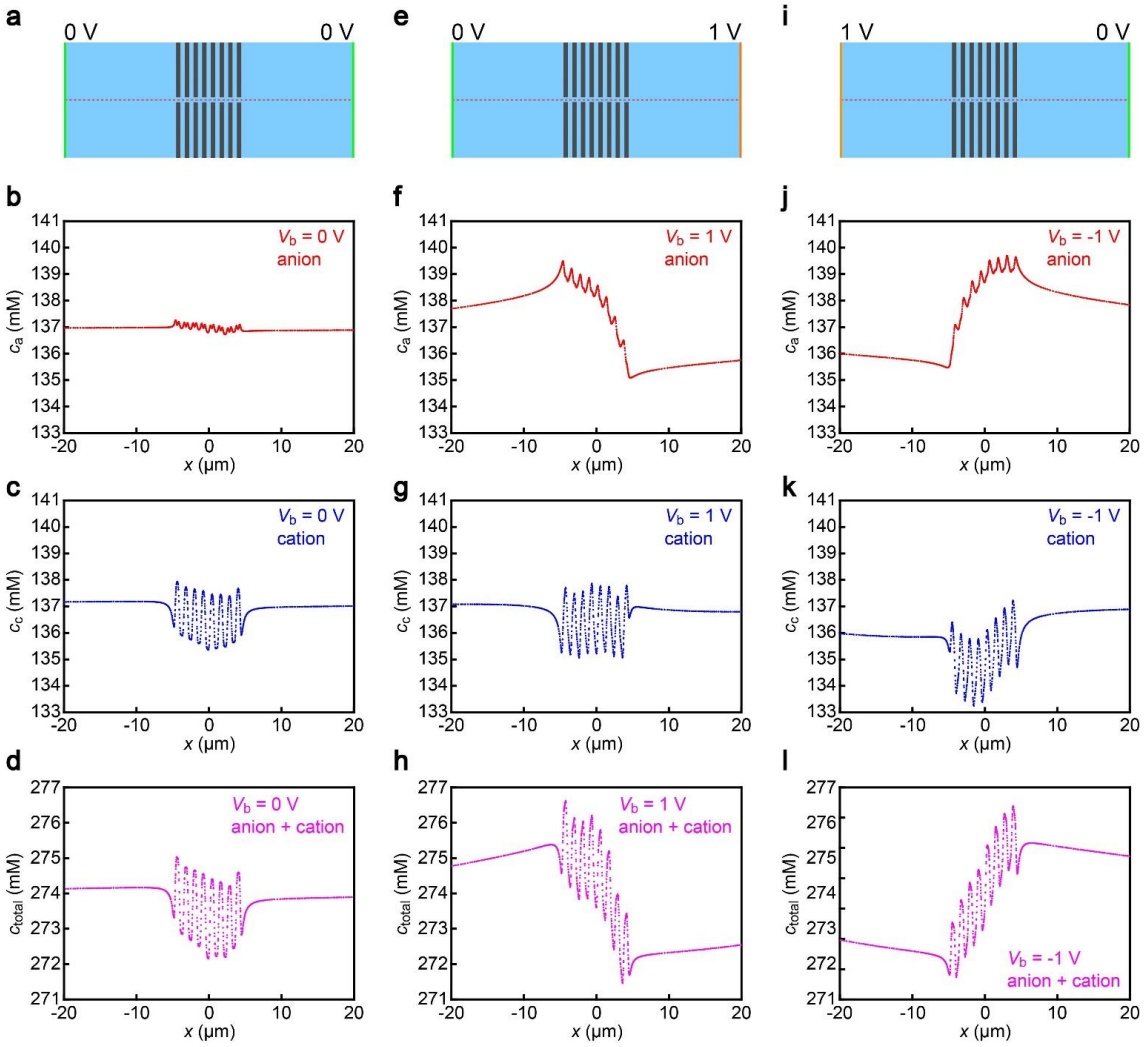

Figure S6. a-d, A schematic model of the octet nanochannel with no voltage applied (a) and the simulated densities of anions (b), cations (c), and both ions (d) along the axial direction *x*. The cation density c_c was slightly higher in the eight constrictions due to the electrostatic attraction to the negatively charged SiO_2 channel wall surface. The anion density c_a is, on the other hand, almost homogeneous throughout the conduit. **e-l,** The ion distributions under the applied voltage of + 1V (e-h) and -1 V (i-l). Under the positive voltage, local density of anions become higher and lower at the left and right sides of the channel (g). In contrast, the effect is reversed under the negative voltage where c_a becomes lower and higher at the left and the right sides (k), which is interpreted as ion concentration polarization induced by the slightly cation selective nature of the SiO_2 nanochannel.[S2] As a result, the ion concentration at the left and right sides is enriched (depleted) and depleted (enriched) under the positive (negative) voltages (h,i) although the change is quite small amounting less than 2 % of the bulk concentration.

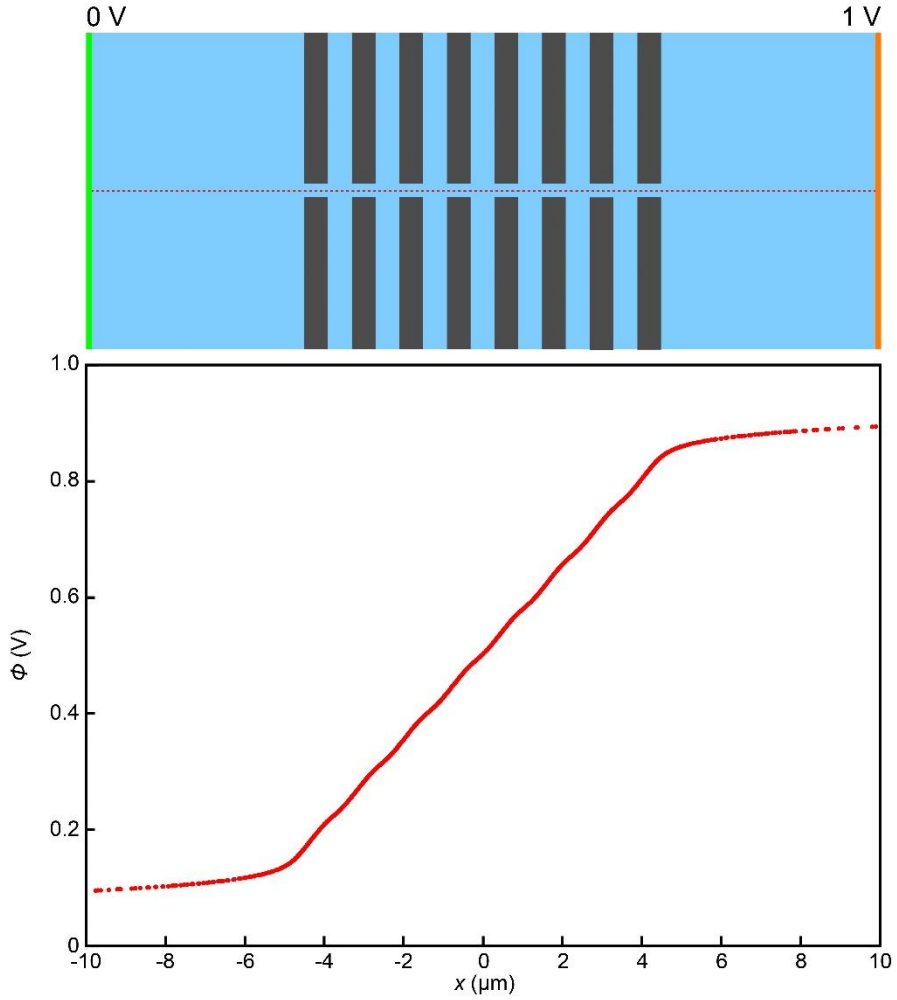

Figure S7. Electric potential profile along the axial direction of the octet nanochannel. No clear signs of ion concentration polarization effect were observed due to the relatively large size of the conduit compared to the Debye length.

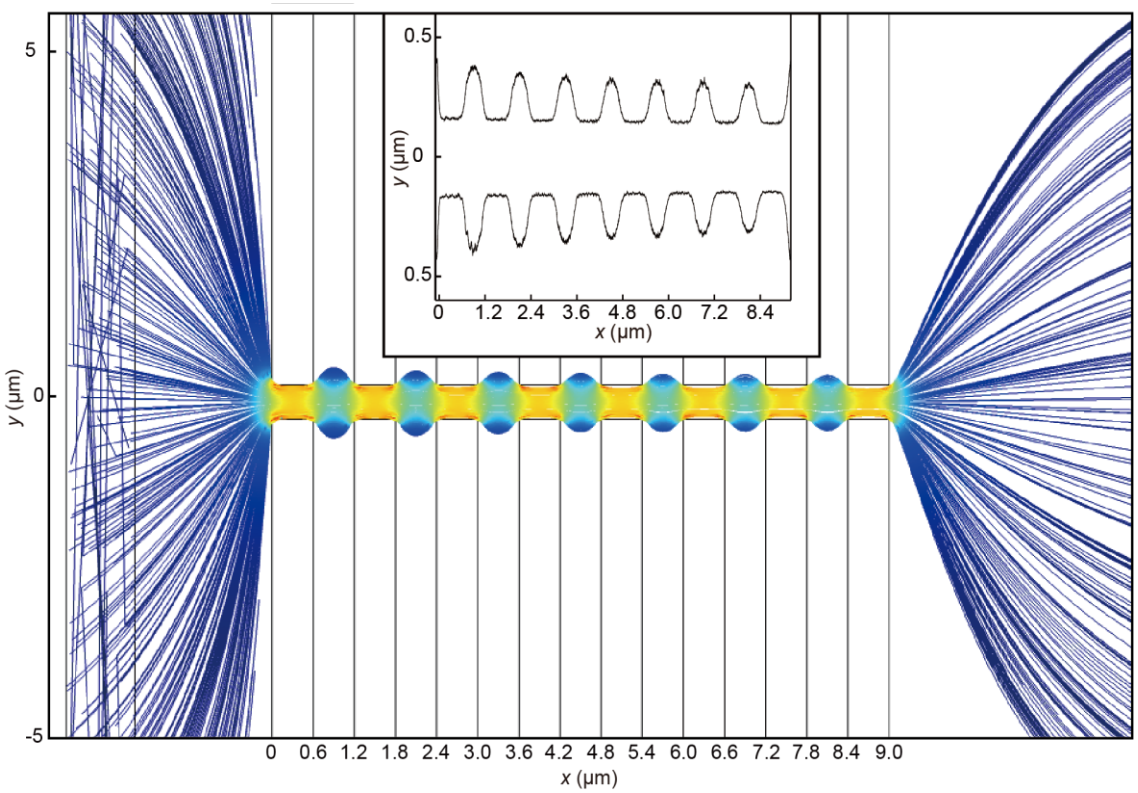

Figure S8. Coarse view of particle trajectories. Inset: Averaged trajectories of the particles moved above and below $y = 0$.

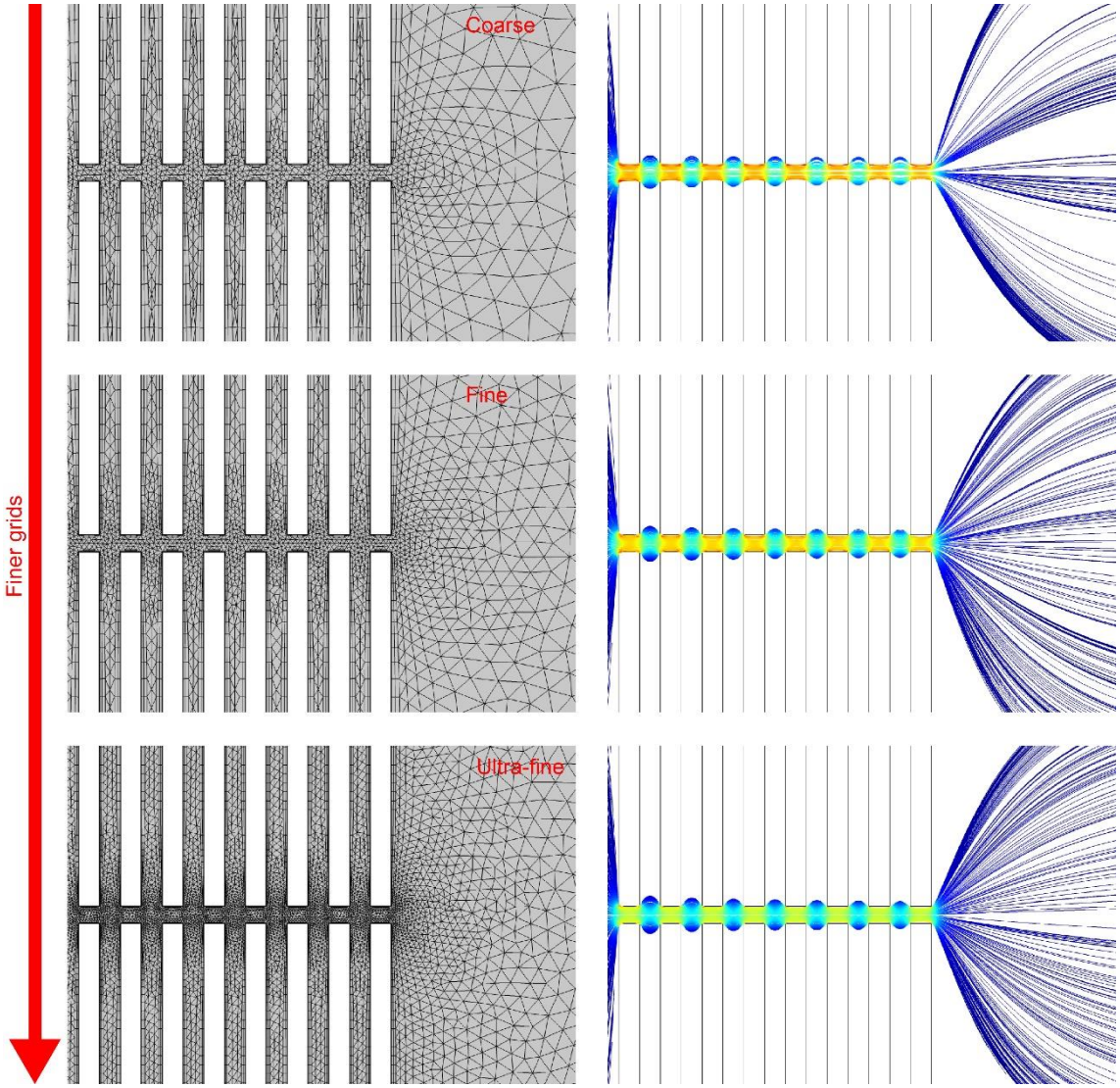

Figure S9. Grid dependence of the finite element analyses. There were no notable difference in the results obtained with the three different mesh sizes. We used the 'Fine' grids to run the simulations.

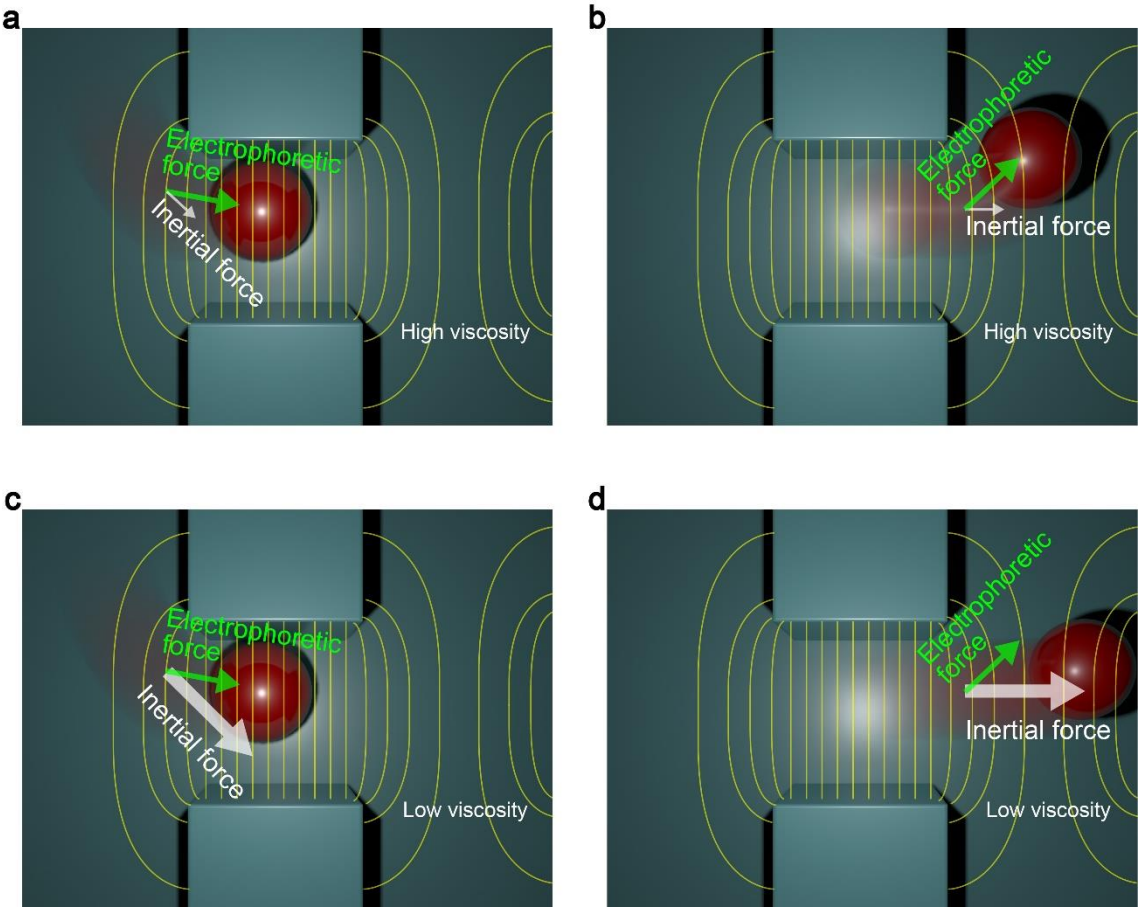

Figure S10. Inertial focusing of nanoparticle electrophoresis in the octet nanochannel. **a,** Particle capture by electric field focused at the narrowed constriction. Yellow lines denote a contour map of the electric potential. The particle speed is low letting the inertial effects to be ineffective to change the direction from that of the electric field. **b,** The particle is accelerated in the strong electric field at the nanoconstriction. When the viscosity of the media is high, however, the motion is rapidly retarded by the viscous drag after getting out the narrowed region since the electric field is relatively weak at there. In this case, the particle moves along the potential gradient that results in the wavy trajectories depicted in Figs. 3d and S4. **c,** On the other hand, the particle moves much faster under a low viscosity condition (c). Therefore, the viscous dragging is insufficient to settle the motion into steady-state due to the short relaxation time. As a result, the particle moves more to the center by inertia compared to the case in (a). **d,** The thing is similar during the escape from the channel where the inertial force, now directing toward the channel axis, brings the particle more to that direction. As these processes repetitively occur eight times in the octet nanochannel, it gives rise to focusing of the nanoparticles at the downstream.

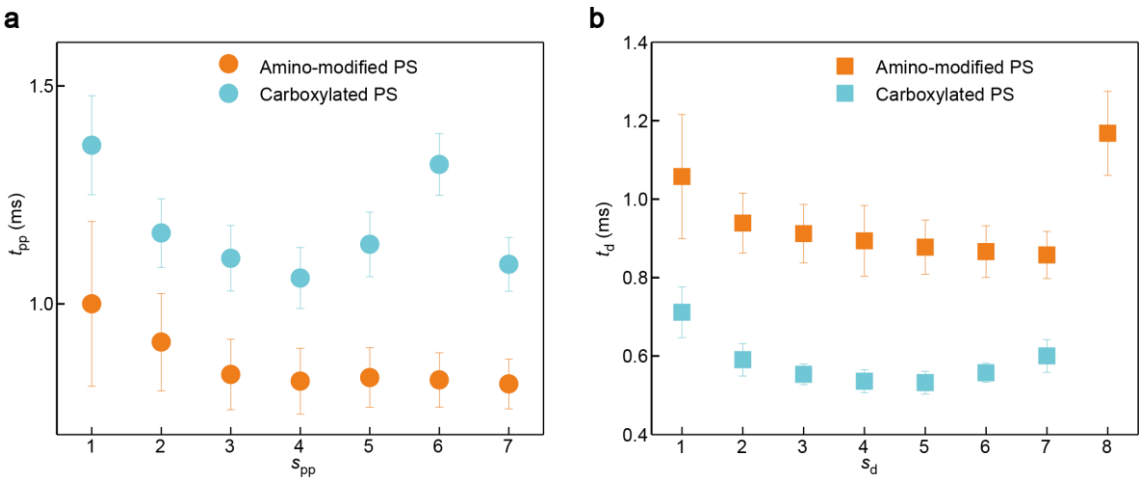

Figure S11. Average Translocation time of amino-modified and carboxylated nanoparticles. a, t_{pp} plotted as a function of *m*. **b,** t_d plotted as a function of *n*. The anomalous 6th t_{pp} of the carboxylated polystyrenes is presumably due to fabrication error in the size of the 6th nano-constriction.

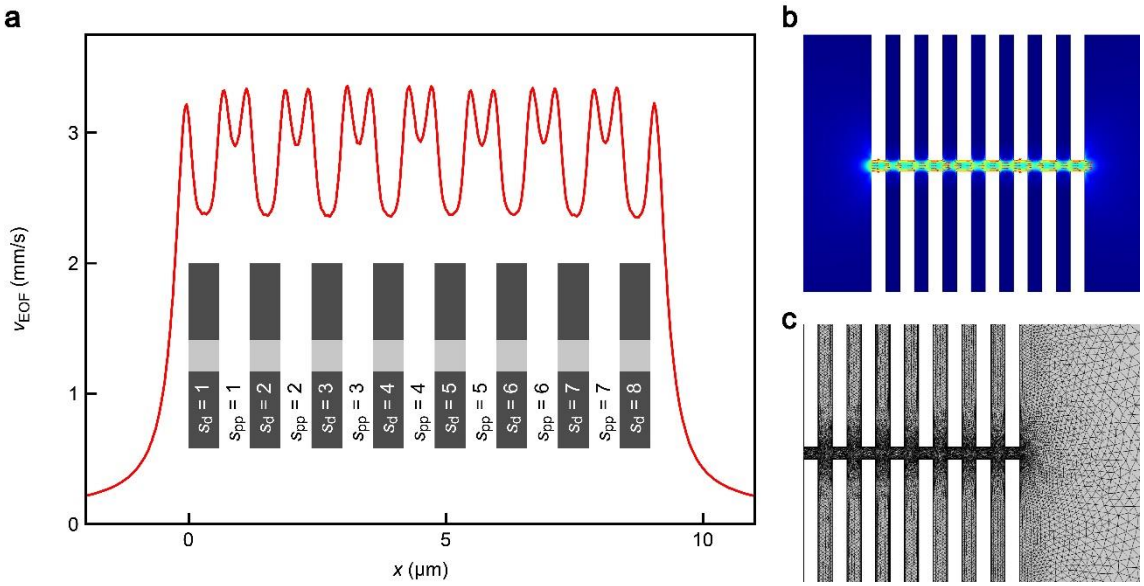

Figure S12. Electroosmotic flow velocity v_{EOF} in the octet nanochannel. **a,** v_{EOF} is around 3 mm/s, which is more than an order of magnitude lower than the electrophoretic speed of the particles estimated by the finite element calculations (Fig. 4i). Meanwhile, we note that this flow velocity is faster than the translocation speed of the particles deduced from the channel length and the resistive pulse widths, which is around 0.8 mm/s. This is presumably a consequence of a discrepancy between the bulk properties assumed in the numerical simulations and the actual conditions in the experiments, such as viscosity for example. In this context, it is noticeable that the particle motions were also overestimated in the simulations (Fig. 4i). Therefore, v_{EOF} should not be compared with the experimental results as it is valid only within the framework of the numerical analyses. **b,** Color map of v_{EOF}. The flow speed is high at the nanochannel wall surfaces. **c,** The model used for the electroosmotic flow speed calculations. The meshes were made finer at the wall surface to accurately simulate the counterion motions.

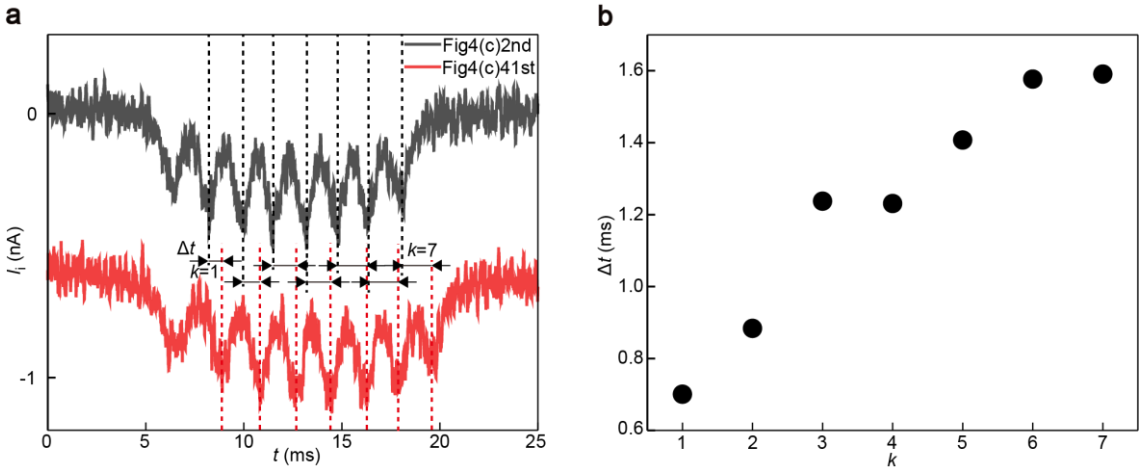

Figure S13. Resistive pulse waveforms. a, Comparison of two resistive pulse signals obtained at the beginning (gray) and after several hours of the ionic current measurement. Δ*t* denote the time between the k_{th} ionic current dips between the two pulses. **b,** Plots of Δ*t* as a function of *k*. The linear increase in Δ*t* indicates the difference in the electrophoretic mobility of the two particles in (a).

Supplementary References

S1. M. Tsutsui, Y. He, K. Yokota, A. Arima, S. Hongo, M. Taniguchi, T. Washio and T. Kawai, *ACS Nano*, 2016, **10**, 803.

S2. Y.-C. Wang, J. Han, *Lab Chip*, 2008, **8**, 392–394